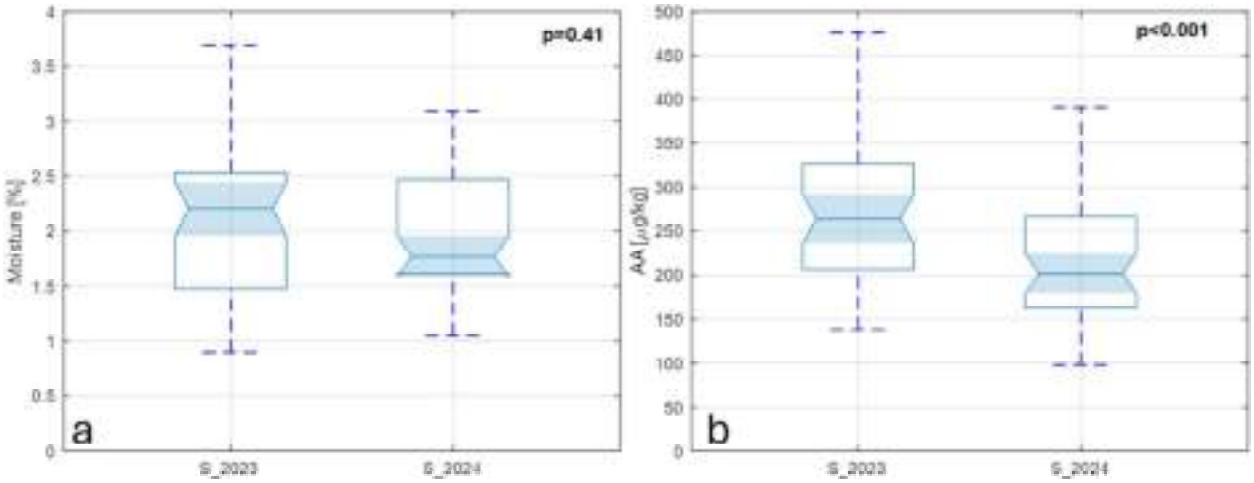

Fig. 4 Moisture (**a**) and acrylamide (**b**) content in biscuit samples from the 2023 (S_2023) and 2024 (S_2024) campaigns, measured with the reference methods. Legend: Boxes show interquartile range; notches indicate 95% Confidence Interval (CI) of the median; whiskers span 1.5 × IQR (Interquartile Range)

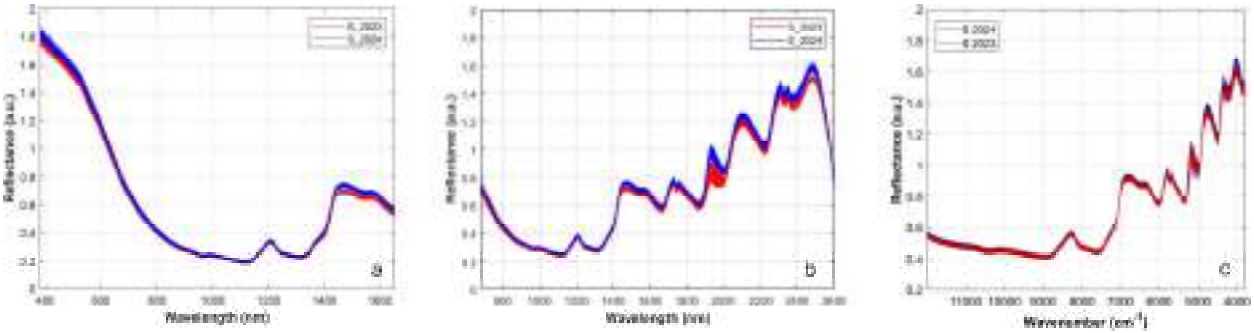

Fig. 5 Spectra of ground biscuits from S_2023 (red) and S_2024 (blue) sampling campaigns acquired using three spectral devices (**a**) D1, (**b**) D2 and (**c**) D3

Results and discussion

Moisture and acrylamide quantification

Figure 4a presents the descriptive statistics of the moisture content measured in biscuit samples collected during the 2023 (S_2023) and 2024 (S_2024) campaigns. The notched box plots display the median, interquartile range, and full data spread for each campaign, with no outliers detected. The two distributions show comparable central tendency and variability, and the two-sample t-test did not reject the null hypothesis ($p = 0.41$), indicating no statistically significant difference between years. This suggests that moisture content remained stable across campaigns, confirming that the changes in production factors did not affect biscuit water content.

The AA concentrations determined by LC–MS/MS ranged approximately from 100 to 500 µg/kg, with mean and median values around 250 and 200 µg/kg, respectively, for both campaigns (Fig. 4b). The observed high variability is likely attributable to the changes in process factors during biscuit production. Despite the overall similarity in distribution patterns, the two-sample t-test rejected the null hypothesis at the 99.9% confidence level ($p < 0.001$), statistically indicating a significant decrease in AA levels in 2024. Finally, the SEL, calculated on ten samples repeated in duplicate, was 18.6 µg/kg considering a mean of 290 µg/kg.

Spectral data exploration

Figure 5 shows the absorbance spectra (arbitrary units, a.u.) of ground biscuit samples from S_2023 dataset and S_2024 dataset acquired using the three devices (D1, D2 and D3).

The VNIR spectral signature of the ground biscuits appears in Fig. 5a. In the visible region, a high absorbance was observed, primarily due to the dark color of the cocoa-based matrix, an effect that appeared consistent across both the S_2023 and S_2024 datasets. As the spectrum transitioned into the pure NIR region (from

700 to 1600 nm), the absorption decreased and the typical spectral assignments emerged, associated with overtones and combination bands of molecular vibrations such as O–H, C–H, and N–H bonds well-known in food matrices to originate from water, lipids, and proteins, respectively (Cen & He, 2007; Williams & Norris, 2001). These spectral features exhibited variations in intensity between the two datasets, suggesting differences in the chemical composition or physical properties. A variation appeared at around 1400—1600 nm, likely reflecting differences in moisture content and water molecule binding to polar sites, given the strong sensitivity of the NIR region to O–H vibrational first overtone (Osborne et al., 1993). This interpretation is also consistent with the different storage conditions applied to the samples, i.e., non-hermetic packaging in S_2023 versus vacuum sealing in S_2024.

D2 (Fig. 5b) spans from a small portion of the visible region to the pure NIR range, which is characterized by multiple broad and overlapping absorption bands. The spectrum shape in the overlapping range between D1 and D2 (around 650—1600 nm) was consistent across both devices. Then, the spectral region from approximately 1400 to 1900 nm displayed well-defined features that can be attributed to the O–H stretching vibrations (centered around 1450 nm) and O–H combination band again closely linked to moisture content and binding (Cen & He, 2007; Cozzolino & Murray, 2004). Within the same region, bands around 1730–1760 nm were consistent with combination bands of C–H stretching and deformation vibrations, typically associated with lipid and carbohydrate fractions (Alamprese et al., 2013). A distinct absorption feature near 1930 nm was commonly attributed to O–H stretching and bending combinations, making it a strong marker of water content and hydration (Williams & Norris, 2001). In the 2300–2500 nm range, further absorption bands appeared, attributed to the combination bands of C–H, N–H, and C=O groups. Bands between 2310–2340 nm were characteristic of C–H combination bands of lipids, while the range 2440–2480 nm included contributions from amide-related N–H vibrations, reflecting protein content (Alamprese et al., 2013; Cozzolino & Murray, 2004). While the overall spectral trends between the S_2023 (red) and S_2024 (blue) datasets remained comparable, differences in band intensity and shape were observed, particularly in moisture-sensitive regions. The slightly higher absorbance observed in the S_2023 spectra (notably at 1450 and 1930 nm) further supported the interpretation of variation in water content and binding, linked to the less controlled storage conditions of that campaign.

Figure 5c describes the absorbance spectra collected using D3. The spectra from both years closely overlapped across most of the range, confirming the consistency of spectral acquisition protocols and sample preparation. However, a difference appeared beyond 7100 cm^{-1} (approximately 1400 nm), corresponding to the strong water absorption band, supporting the hypothesis of a different water content and binding with the other molecules. The general spectral profile was consistent with D2 and D1.

Overall, the spectral data demonstrated a high degree of reproducibility and consistency across the two sampling campaigns. However, differences appeared between the spectral signatures of samples stored in the two different packaging systems. These variations primarily reflect changes in the absorption of O–H bonds, particularly around 1445 nm and 1940 nm. Interestingly, the S_2023 dataset, comprising samples stored without vacuum sealing, showed lower absorbance than S_2024 dataset in the spectral regions most affected by water, and a shift in the band maxima. This apparently counterintuitive result could be justified by three main phenomena: (1) baseline shifts and scattering effects, (2) change from bound to free water, (3) matrix reorganization. In detail, in diffuse-reflectance VNIR, the detected light depends not only on molecular absorption but also on how much light is scattered and reflected (Mancini et al., 2019). When a low-moisture sample ages, it absorbs environmental humidity and loses crispness, its microstructure changes, and so the absorbance-like reflectance does. Furthermore, as water moves from tightly bound sites to freer states, the O–H absorption bands broaden and shift, sometimes reducing the peak intensity in the typical water regions (Tsenkova, 2009). Finally, structural changes in the food matrix, such as starch retrogradation or protein network rearrangement, modify both light penetration and water interactions, resulting in shifts of band maxima and altered spectral intensity (Mancini et al., 2019).

After raw spectra visualization, different spectral transformations were evaluated (Savitzky-Golay smoothing, SNV, Detrending, and Savitzky-Golay first and second derivative) for PCA exploration. By the end of the iterative process, SNV was applied to the D1 dataset. Instead, since the D2 spectral data showed a constant linear offset (baseline shifts) along the entire spectral range, a detrending preprocessing was performed giving a mean intensity of zero for each spectrum. Lastly, SNV combined with smoothing (Savitzky-Golay, 15 data point window, 3rd polynomial order) was applied to the D3 dataset to minimize offsets and global intensity effects (Roger et al., 2022).

Those pretreatments allowed a slight differentiation of samples according to AA concentration in the plane defined by PC1 vs PC3, as shown in Fig. 6a, representing the score plot developed for NIR spectra acquired with

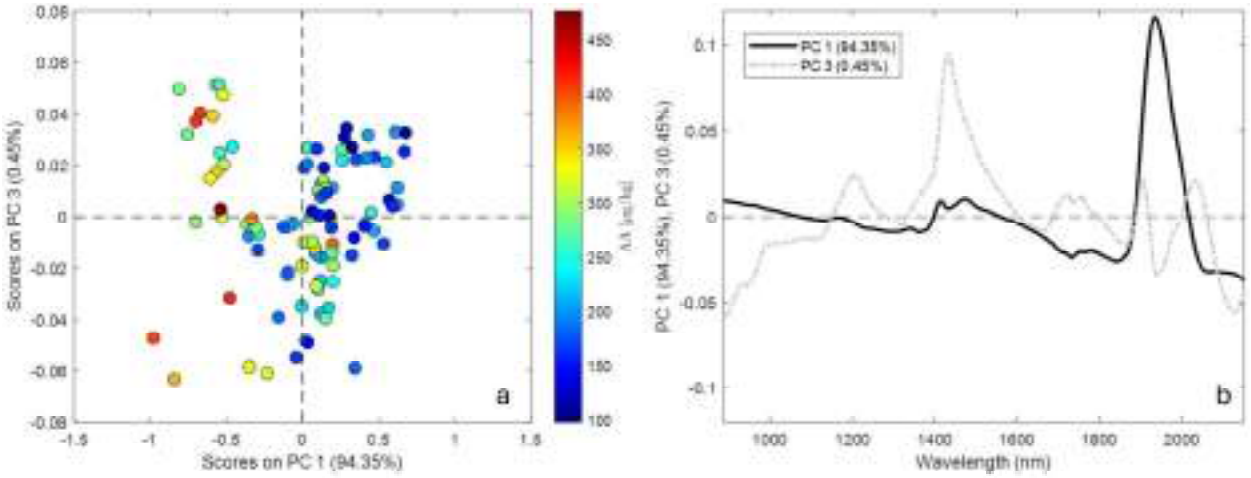

Fig. 6 PCA score plot (**a**) and loading plot (**b**) of NIR spectra acquired with the D2 device on ground biscuit samples from the S_2023 and S_2024 campaigns. In the score plot, samples are colored according to AA content

the D2 device for ground biscuit samples of the 2023 and 2024 campaigns.

Samples with low AA concentration are mainly distributed at positive PC1 scores due to high positive weight of signals at 1940 nm in PC1, and 1200 nm and 1433 nm in PC3 (Fig. 6b), related to O–H stretching and bending combinations, and O–H vibrational first overtone (Workman & Weyer, 2007). On the other hand, samples characterized by high AA content (> 350 µg/kg) are more frequently positioned at negative PC1 scores where the loads of the region around 1800 nm are relevant.

Modelling

Table 1 provides a comprehensive evaluation of predictive model performances for the three spectroscopic devices (D1, D2, and D3) across the two datasets (S_2023 and S_2024), assessed through calibration and cross-validation. The metrics considered include RMSE, R^2, bias, and RPD. Calibration results showed R^2 values ranging from 0.55 to 0.81, reflecting varying levels of model fit; the S_2024 dataset collected with the D2 device achieved the lowest RMSE (28.42 µg/kg). Bias values across all models were negligible (on the order of 10^{-12} or lower), indicating no significant systematic errors. As expected, model performance decreased slightly after cross-validation, with R^2 values decreasing to 0.42—0.70, and RMSE values increasing. Nevertheless, bias remained low, supporting good model generalization. RPD values ranged from 1.3 to 2.0. According to standard interpretive benchmarks, models based on D1 and D3 for S_2023 (RPD = 2.0) exhibited sufficient predictive quality for quantitative applications, while the D2 models maintained stable and moderately strong performance across both years (RPD = 1.8). In contrast, the lowest RPD values were observed for D1 and D3 on the S_2024 dataset (1.6 and 1.3, respectively), with the latter falling below the threshold typically regarded as acceptable for quantitative modeling.

As mentioned before, the two storage methods induced chemical modifications in the ground biscuit samples. These changes altered the NIR spectral absorption, with consistent deviations observed across all instruments (D1, D2, and D3) from approximately 1400 nm to the upper limit of their detectable spectral range (Fig. 5). As a consequence, the S_2023 and S_2024 datasets presented two different experimental domains, making unfeasible the external validation of the model developed with the S_2023 dataset with the data collected in 2024. The variance related to the two different domains was also highlighted by PCA (Fig. 7).

Figure 7a shows the PCA score plot of data collected with D2, where each point represents a sample projected in the space defined by the first two PCs, which together explained 98.85% of the total variance (PC1 = 94.35%, PC2 = 4.50%). The plot highlighted a clear separation between the samples collected in 2023 and 2024 campaigns, suggesting substantial spectral differences between the two datasets, likely reflecting differences related to sample storage. Indeed, PC1 loadings (Fig. 7b) were characterized by the strong contribution around 1930 nm, a wavelength associated with the combination band of O–H stretching and bending, which is highly sensitive to water content and structure. This suggested that moisture differences were a dominant factor differentiating the two groups. Additional features in the 1400–1500 nm and 2200–2300 nm regions, which also relate to O–H and C–H bonds, further supported this hypothesis. Overall, the

Table 1 Calibration and cross-validation performance metrics of PLS regression models for acrylamide concentration estimation using VNIR and FT-NIR spectra collected with the three devices (D1, D2, D3) on ground biscuit samples of S_2023 and S_2024 campaigns

Device	*Campaign*	*LV*	Calibration			Cross-validation			
			RMSE (µg/kg)	R^2	*Bias*	*RMSE (µg/kg)*	R^2	*Bias*	*RPD*
D1	S_2023	6	32.90	0.81	$6.25e^{-13}$	41.76	0.70	0.003	2.0
	S_2024	8	29.72	0.80	$1.6e^{-12}$	42.76	0.60	0.46	1.6
D2	S_2023	6	36.16	0.77	$-5.7e^{-14}$	45.56	0.65	0.77	1.8
	S_2024	8	28.42	0.81	$1.13e^{-13}$	37.68	0.68	−0.13	1.8
D3	S_2023	3	35.33	0.79	$-5.7e^{-14}$	41.63	0.70	0.17	2.0
	S_2024	4	44.11	0.56	$8.88e^{-16}$	50.79	0.42	−0.001	1.3

LV number of latent variables, *RMSE* root mean square error, R^2 coefficient of determination, *RPD* residual prediction deviation

PCA results revealed that the dominant source of spectral variation between the 2023 and 2024 biscuit samples was linked to storage-related differences (non-hermetic vs vacuum-sealed), as also observed in the raw spectra (Fig. 5).

Calibration transfer and validation

The sample packaging management during the two different campaigns (i.e., not hermetically closed for S_2023 and under vacuum for S_2024) resulted to be an external parameter affecting the spectral information due to differences in chemical composition of biscuits not related to the baking process. To account for this external factor and enable external validation while enhancing model generalizability, EPO preprocessing method was applied. This correction reduces the influence of unwanted spectral variability, such as the changes in water content and distribution, thereby improving the robustness and practical applicability of the models in new domains.

The effectiveness of EPO was evaluated applying the trained model (calibration set constituted by S_2023 data and 25% of S_2024 data) to two independent test sets comprising 25% or 50% of the S_2024 data (named TS_A and TS_B, respectively) not used in the model training phase. TS_A was used to fine-tune the EPO hyperparameters (the selected number of PCs was 12, 12, and 5 for D1, D2 and D3, respectively) by assessing model performance through RMSE and bias metrics. After determining the optimal number of PCs, TS_B was used to evaluate the final performance of the EPO-corrected model.

Figure 8 shows the regression line of the of the PLS models calculated after EPO correction, while Table 2 summarizes the performance of the models in prediction. For each instrument, RMSE and R^2 values for calibration, cross-validation (CV), and external validation are reported, the latter performed using 50% of the S_2024 dataset as an independent test set.

In general, the models showed satisfactory calibration performance, but moderate predictive performance on external data, confirming the challenges in transferring model accuracy across datasets of the two sampling campaigns. Both D1- and D2-based models required 6 LVs, whereas 5 LVs were used in the model calculated with the D3 dataset. The R^2 in calibration ranged from 0.80 to 0.87, but it dropped to 0.59—0.76 in cross-validation, and further to 0.43—0.53 in external prediction. In particular, the model constructed with the D2 dataset showed in prediction the lowest R^2 and the highest bias (18.3 µg/kg) and RMSE (53.8 µg/kg), suggesting higher sensitivity to domain variability. Models developed with D1 and D3 datasets showed more stability, with lower bias in prediction. The best predictive performance was obtained with the D3 dataset with the highest R^2 (0.53) and the lowest RMSE (39.1 µg/kg). In any case, the obtained RMSE in prediction was slightly more than twice the SEL (18.6 µg/kg), indicating suitability for rapid screening and process feedback (Ciurczak et al., 2021).

Applicability—envisioning industrial implementation of NIR systems for acrylamide monitoring in the food industry

AA must be tightly controlled in industrial food production to ensure food safety and regulatory compliance. Real-time or at-line NIR monitoring offers rapid, non-destructive analysis that far outpaces the time-consuming sample preparation and lengthy turnaround of traditional laboratory assays. In literature, extensive work has been done on potato chips and French fries (Adedipe et al., 2016; Ayvaz & Rodriguez-Saona, 2015; Peraza-Alemán et al., 2025; Skinner et al., 2021; Smit et al., 2025; Xie et al., 2023), whereas there is a lack of application for other food matrices.

The first study by Ayvaz and Rodriguez-Saona (2015) considered both benchtop and handheld instruments, however the potato chips were pretreated to obtain a "chip cake", i.e., chips were blended, and oil was expelled by a hydraulic press. Thus, the sample preparation

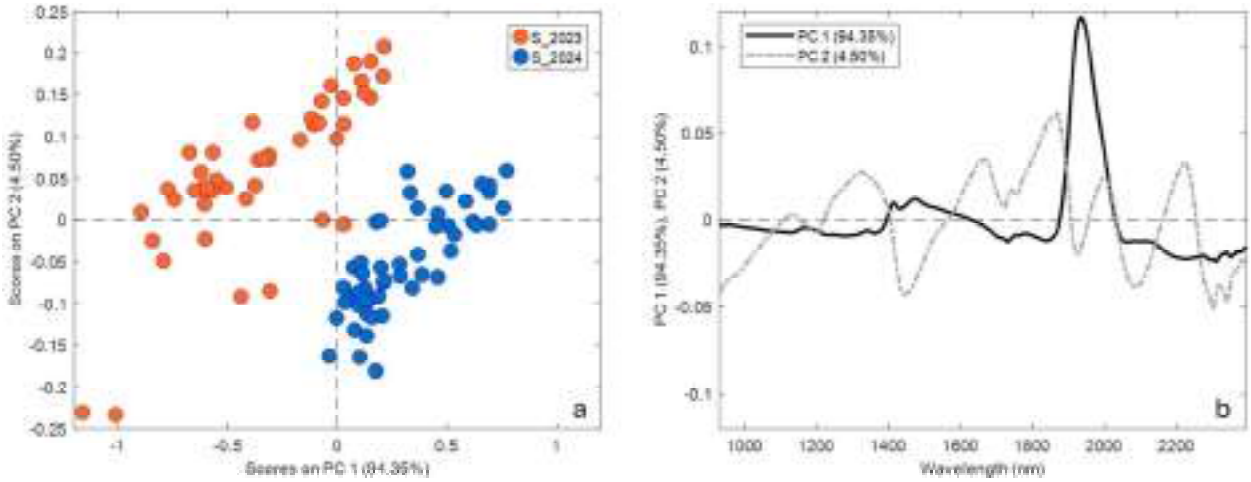

Fig. 7 PCA score plot (**a**) and loading plot (**b**) of NIR spectra acquired with the D2 device on ground biscuit samples from the S_2023 and S_2024 campaigns

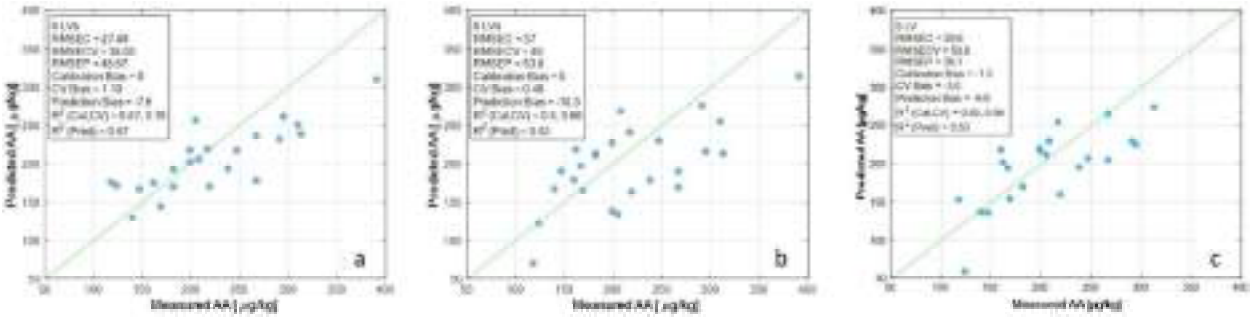

Fig. 8 EPO-PLS regression lines for acrylamide concentration prediction in cocoa biscuits, calculated using the data collected with the three spectral devices (**a**) D1, (**b**) D2 and (**c**) D3

procedure makes the approach far from a process line application. Furthermore, a higher error in prediction (78 µg/kg) was obtained compared to the RMSEP (47.69 µg/kg) obtained in a more recent study (Xie et al., 2023). This could be linked to the AA content in commercial chips (169 to 2453 µg/kg) analyzed by Ayvaz and Rodriguez-Saona (2015), compared to the chips analyzed by Xie et al. (2023) with AA levels (56.7—789.0 µg/kg) in line with EU limitation for this type of products (750 µg/kg). Indeed, the PLS prediction results obtained by Xie et al. (2023) are in line with the regression models presented in this study, having RMSE in prediction ranging from 39.1 to 53.8 µg/kg depending on the considered instrument.

However, the NIR solutions proposed in the potato chip studies revised from the literature are limited due to sample preparation. Indeed, an industrial implementation

Table 2 Figures of merit of EPO-PLS regression models for acrylamide concentration prediction in cocoa biscuits using VNIR and FT-NIR spectra collected with the three devices (D1, D2, D3)

Device	*LV*	Calibration			Cross-validation			Prediction		
		RMSE (µg/kg)	R^2	*Bias*	*RMSE (µg/kg)*	R^2	*Bias*	*RMSE (µg/kg)*	R^2	*Bias*
D1	6	27.49	0.87	0	38.02	0.76	1.19	48.87	0.47	−7.6
D2	6	37.00	0.80	0	49.00	0.66	0.46	53.80	0.43	−18.3
D3	5	29.80	0.85	−1.3	50.80	0.59	−3.0	39.10	0.53	−9.6

Table 3 Spectral devices specifications

	Application	Spectral range (nm)	Minimum spectral resolution	Measuring distance	Sample presentation
D1 (ZEISS, Corona Process)	*On-line/in-line*	380—1650	≤ 10 nm (FWHM)	100–590 mm	Measures solid and powdered samples in absorbance mode
D2 (Spectra star, Unity)	*At-line*	680—2600	10.0 ± 0.3 nm (FWHM)	contact	Optimized for solid, granular, and powdered samples, using a rotating sample cup for improved homogeneity
D3 (FT-NIR Bruker Optics, MPA)	*Off-line/at-line/in-line*	800—2500	2 cm^{-1} (FT)	contact	Supports solids, powders, and liquids, with measurement via reflection, transmission, or fiber-optic probe integration

* *FWHM* Full Width at Half Maximum

able to deal with intact products along the conveyor belt would be necessary. Results obtained from intact product analyses were presented by Peraza-Alemán et al. (2025), who developed a hyperspectral imaging (HSI) method for AA prediction in potato chips by PLS modelling, reaching a RMSE in prediction of 201 µg/kg when considering a wide AA range (from 201 to 2548 µg/kg). HSI systems take advantage of spatial information, thus generating pixel-level maps of surface AA distribution. However, they are highly affected by environmental fluctuations in the industrial setting, and they require long spectral acquisition times.

The instrumental solutions proposed in this study, even if tested on ground biscuits, were selected for their possible use for at-line/in-line implementation (Table 3). The D3 instrument was equipped with an integrating sphere and a rotating sample module, as this was considered the best method for analyzing ground samples over the full NIR spectral range (12,500–4000 cm^{-1} or 800–2500 nm) in absorbance mode. The actual setup was characterized by a total acquisition time around 30 s, with 32 scans and 8 cm^{-1} resolution. However, the main advantage of D3 is its versatility, which allows, for instance, for punctual analysis of solid samples by fiber optic probes. Furthermore, reducing the spectral range, the number of scans and the resolution, a lower acquisition time (≈ 10 s) could be reached while guaranteeing the optimal measurement conditions (Grassi et al., 2021). D2 was tested as an at-line NIR solution for the analyses of ground samples placed in a rotating Petri dish. The instrument operated in absorbance mode over 680–2600 nm, and enabled to acquire a spectrum every 10 s. Both D2 and D3 could be suitable for intact biscuit analysis for at-line solutions, because mounting them above the conveyor belt will probably not succeed in achieving the correct configuration with the necessary standoff distance. Among the selected instruments, D1 seems to be the most suitable for in-line implementation as developed for absorbance measurements with a working distance between 80 and 600 mm. In the presented case the spectral acquisition was performed in absorbance mode using a 60 mm illumination spot and measuring at a fixed sensor-to-sample distance of 150 mm. However, different settings could be reached for industrial implementation. Moreover, D1 guarantees rapid spectral acquisition, with a total acquisition time of around 2 s. Thus, future work on the industrial implementation would need to face proper integration of VNIR sensors considering precise alignment of the sensor head at an optimal distance from intact biscuit moving on the conveyor belt.

Over the need for distance measurement capabilities and fast acquisition time, the industrial implementation should consider synchronized sampling frequency and data modelling throughput to match line speed. Finally, robust housing or compensation algorithms are mandatory to mitigate environmental fluctuations, such as temperature or humidity changes, as demonstrated by the performance improvement obtained by EPO correction.

Conclusions

This study evaluated the feasibility of using VNIR and FT-NIR spectroscopy as a screening system for AA quantification in industrially produced cocoa-based biscuits. By the development of machine learning models based on spectral data collected with three distinct instruments (D1, D2, and D3) and across two independent sampling campaigns (S_2023 and S_2024), the research addressed both analytical performance and storage condition effects on model performances.

The biscuit formulation and baking set up successfully captured a wide range of AA concentrations, creating a representative and challenging dataset for model

development. Across all instruments, PLS regression models showed promising predictive performance in cross-validation, with R^2 values ranging from 0.65 to 0.87 and RPD values generally above 1.5. These results confirmed the models' suitability for semi-quantitative applications and trend monitoring. However, external validation revealed domain shifts between datasets collected in 2023 and 2024, likely caused by differences in sample packaging before storage (i.e., non-hermetic vs vacuum-sealed packaging). PCA confirmed that storage-related variability, particularly affecting O–H bond absorptions, was the dominant factor contributing to spectral differences. To overcome this challenge and ensure model transferability, EPO was applied. The EPO correction improved model robustness and enabled acceptable external predictive performance ($R^2 \sim 0.43$–0.47; RMSE ~ 49–54 μg/kg), despite intrinsic matrix variability.

Overall, the results support the integration of VNIR/FT-NIR spectroscopy into industrial quality control workflows as a PAT tool for AA monitoring. While not yet a substitute for reference methods in regulatory compliance, VNIR/FT-NIR spectroscopy can provide rapid screening and process feedback, contributing to a QbD approach. Future work will focus on expanding the calibration dataset to include additional product types, processing conditions, and production lines, thereby enhancing model generalization and facilitating real-time application in dynamic manufacturing environments. Furthermore, the results presented in this work should be regarded as a proof-of-concept demonstrating basic AA detectability under ideal conditions. The extension to intact biscuit detection is a critical next step, and future work will focus on validating the model using intact biscuits under simulated or real in-line conditions, including varying orientations and conveyor speeds. Incorporating these factors will allow the development of more robust models tailored for industrial deployment.

Authors' contributions

A.T.: Conceptualization, Data curation, Investigation, Methodology, Software, Validation, Visualization, Investigation, Writing – original draft, Writing – review and editing. S.G.: Conceptualization, Data curation, Investigation, Methodology, Validation, Visualization, Writing – original draft, Writing – review and editing. R.B.: Conceptualization, Data curation, Formal analysis, Investigation, Methodology, Validation, Visualization, Writing – review and editing. V.S.: Data acquisition, Resources, Data curation, Writing – review and editing. I.L.: Data acquisition, Formal analysis, Software. C.P.: Resources, Supervision, Validation. R.G.: Supervision, Project administration. M.S.: Conceptualization, Methodology, Project administration, Supervision, Writing – review and editing. C.A.: Conceptualization, Supervision, Project administration, Methodology, Formal analysis, Visualization, Writing – original draft, Writing – review and editing V.G.: Conceptualization, Data curation, Investigation, Methodology, Resources, Supervision, Validation, Project administration, Writing – review and editing.

Funding

The authors acknowledge support from the University of Milan through the APC initiative.

Data availability

On request.

Declarations

Ethics approval and consent to participate

Not applicable. The present work does not involve the use of animal or human subjects.
The present work does not involve chemicals, procedures or equipment that have any unusual hazards inherent in their use.

Consent for publication

All authors agreed with the publication in this journal.

Competing interests

The authors declare no competing interests.

Author details

[1]Department of Agricultural and Environmental Sciences (DiSAA), Università Degli Studi Di Milano, Milan, Italy. [2]Department of Food, Environmental, and Nutritional Sciences (DeFENS), Università Degli Studi Di Milano, Milan, Italy. [3]Barilla G.R. F.lli SpA, Research, Development & Quality, Global Bakery Process & Technology Development, Parma, Italy. [4]Barilla G.R. F.lli SpA, Research, Development & Quality, Sensory and Analytical Food Science, Parma, Italy. [5]Department of Food and Drug, University of Parma, Parma, Italy.

Received: 25 February 2026 Accepted: 28 April 2026
Published online: 6 June 2026

References

Adedipe, O. E., Johanningsmeier, S. D., Truong, V. D., & Yencho, G. C. (2016). Development and validation of a near-infrared spectroscopy method for the prediction of acrylamide content in French-fried potato. *Journal of Agricultural and Food Chemistry,64*(8), 1850–1860. https://doi.org/10.1021/acs.jafc.5b04733

Alamprese, C., Casale, M., Sinelli, N., Lanteri, S., & Casiraghi, E. (2013). Detection of minced beef adulteration with turkey meat by UV–vis, NIR and MIR spectroscopy. *LWT-Food Science and Technology,53*(1), 225–232. https://doi.org/10.1016/j.lwt.2013.01.027

Ayvaz, H., & Rodriguez-Saona, L. E. (2015). Application of handheld and portable spectrometers for screening acrylamide content in commercial potato chips. *Food Chemistry,174*, 154–162. https://doi.org/10.1016/j.foodchem.2014.11.001

Becalski, A., Brady, B., Feng, S., Gauthier, B. R., & Zhao, T. (2011). Formation of acrylamide at temperatures lower than 100 C: The case of prunes and a model study. *Food Additives and Contaminants,28*(6), 726–730. https://doi.org/10.1080/19440049.2010.535217

Calbiani, F., Careri, M., Elviri, L., Mangia, A., & Zagnon, I. (2004). Development and single-laboratory validation of a reversed-phase liquid chromatography–electrospray–tandem mass spectrometry method for identification and determination of acrylamide in foods. *Journal of AOAC International,87*(1), 107–115. https://doi.org/10.1093/jaoac/87.1.107

Cen, H., & He, Y. (2007). Theory and application of near infrared reflectance spectroscopy in determination of food quality. *Trends in Food Science & Technology,18*(2), 72–83. https://doi.org/10.1016/j.tifs.2006.09.003

Ciurczak, E. W., Igne, B., Workman Jr, J., & Burns, D. A. (Eds.). (2021). *Handbook of near-infrared analysis*. CRC press.

Cozzolino, D., & Murray, I. (2004). Identification of animal meat muscles by visible and near infrared reflectance spectroscopy. *LWT-Food Science and Technology,37*(4), 447–452. https://doi.org/10.1016/j.lwt.2003.10.013

EU-funded HEATOX project (2003–2007). (2007). *Press release: HEATOX project completed—brings new pieces to the acrylamide puzzle*. Livsmedelsverket, pp. 9–19.

European Commission (EU). (2017). Commission regulation 2017/2158 of 20 November 2017 establishing mitigation measures and benchmark levels for the reduction of the presence of acrylamide in food. *Official Journal of the European Union*, 304, 24–44.

European Food Safety Authority (EFSA). (2012). Update on acrylamide levels in food from monitoring years 2007 to 2010. *EFSA Journal*, 10(10). https://doi.org/10.2903/J.EFSA.2012.2938

Gökmen, V., & Senyuva, H. Z. (2006). Study of colour and acrylamide formation in coffee, wheat flour and potato chips during heating. *Food Chemistry,99*(2), 238–243. https://doi.org/10.1016/j.foodchem.2005.07.057

Gökmen, V., Açar, Ö. Ç., Arribas-Lorenzo, G., & Morales, F. J. (2008). Investigating the correlation between acrylamide content and browning ratio of model cookies. *Journal of Food Engineering,87*(3), 380–385. https://doi.org/10.1016/j.jfoodeng.2007.12.028

Grassi, S., & Alamprese, C. (2018). Advances in NIR spectroscopy applied to process analytical technology in food industries. *Current Opinion in Food Science,22*, 17–21. https://doi.org/10.1016/j.cofs.2017.12.008

Grassi, S., Strani, L., Alamprese, C., Pricca, N., Casiraghi, E., & Cabassi, G. (2021). A FT-NIR process analytical technology approach for milk renneting control. *Foods,11*(1), Article 33. https://doi.org/10.3390/foods11010033

Hu, Q., Xu, X., Fu, Y., & Li, Y. (2015). Rapid methods for detecting acrylamide in thermally processed foods: A review. *Food Control,56*, 135–146. https://doi.org/10.1016/j.foodcont.2015.03.021

International Agency for Research on Cancer (IRAC). (1994). Some industrial chemicals. *IRAC Monographs on the Evaluation of Carcinogenic Risk for Chemicals to Humans*, *60*, 435. IRAC, Lyon, France.

Keramat, J., Lebail, A., Prost, C., & Jafari, M. (2011). Acrylamide in baking products: A review article. *Food and Bioprocess Technology,4*(4), 530–543. https://doi.org/10.1007/s11947-010-0495-1

Mancini, M., Toscano, G., & Rinnan, Å. (2019). Study of the scattering effects on NIR data for the prediction of ash content using EMSC correction factors. *Journal of Chemometrics,33*(4), Article e3111. https://doi.org/10.1002/cem.3111

Medina-Orjuela, M. E., Barrios-Rodríguez, Y. F., Carranza, C., Amorocho-Cruz, C., Gentile, P., & Girón-Hernández, J. (2024). Enhancing analysis of neoformed contaminants in two relevant food global commodities: Coffee and cocoa. *Heliyon,10*(10), Article e31506. https://doi.org/10.1016/J.HELIYON.2024.E31506

Naes, T., & Isaksson, T. (1991). How should SEL be defined? *NIR News,2*, 16–16. https://doi.org/10.1255/nirn.60

Oliveri, P., Malegori, C., Mustorgi, E., & Casale, M. (2020). Application of chemometrics in the food sciences. *Comprehensive Chemometrics (Second Edition),4*, 99–111. https://doi.org/10.1016/B978-0-12-409547-2.14748-1

Osborne, B. G., Mertens, B., Thompson, M., & Fearn, T. (1993). The authentication of Basmati rice using near infrared spectroscopy. *Journal of near Infrared Spectroscopy,1*(2), 77–83.

Patel, D., Bhise, S., Kapdi, S. S., & Bhatt, T. (2024). Non-destructive hyperspectral imaging technology to assess the quality and safety of food: A review. *Food Production, Processing and Nutrition,6*(1), 69. https://doi.org/10.1186/s43014-024-00246-4

Peraza-Alemán, C. M., López-Maestresalas, A., Jarén, C., de Galarreta, J. I. R., Barandalla, L., & Arazuri, S. (2025). Mapping acrylamide content in potato chips using near-infrared hyperspectral imaging and chemometrics. *Food Chemistry,479*, Article 143794. https://doi.org/10.1016/j.foodchem.2025.143794

Pérez-Beltrán, C. H., Jiménez-Carvelo, A. M., Torrente-López, A., Navas, N. A., & Cuadros-Rodríguez, L. (2023). QbD/PAT-state of the art of multivariate methodologies in food and food-related biotech industries. *Food Engineering Reviews,15*, 24–40. https://doi.org/10.1007/s12393-022-09324-0

Roger, J. M., Chauchard, F., & Bellon-Maurel, V. (2003). EPO–PLS external parameter orthogonalisation of PLS application to temperature-independent measurement of sugar content of intact fruits. *Chemometrics and Intelligent Laboratory Systems,66*(2), 191–204. https://doi.org/10.1016/S0169-7439(03)00051-0

Roger, J. M., Mallet, A., & Marini, F. (2022). Preprocessing NIR spectra for aquaphotomics. *Molecules,27*(20), Article 6795. https://doi.org/10.3390/MOLECULES27206795

Rydberg, P., Eriksson, S., Tareke, E., Karlsson, P., Ehrenberg, L., & Törnqvist, M. (2005). Factors that influence the acrylamide content of heated foods. *Advances in Experimental Medicine and Biology,561*, 317–328. https://doi.org/10.1007/0-387-24980-X_24

Sepehr, A., Carraro, A., Napoli, M., Pescatore, A., & Guerrini, L. (2026). Non-destructive acrylamide quantification in whole-grain bread using RGB-thermal images. *European Food Research and Technology,252*(2), 73. https://doi.org/10.1007/s00217-025-04972-y

Skinner, M. M., Seale, J. T., Cantrell, M. S., Collins, J. M., Turner, M. W., & McDougal, O. M. (2021). Instrumentation for routine analysis of acrylamide in French fries: Assessing limitations for adoption. *Foods,10*(9), Article 2038. https://doi.org/10.3390/foods10092038

Smit, I., Vosmann, K., Weber, L., Truberg, B., Muders, K., Bülbül, M. K., Demeril, U., Çalışkan, M. E., & Haase, N. U. (2025). Potential of near-infrared spectroscopy (NIRS) for prediction of acrylamide formation in French fries in the potato breeding process. *Food Chemistry,463*, Article 141214. https://doi.org/10.1016/j.foodchem.2024.141214

Tareke, E., Rydberg, P., Karlsson, P., Eriksson, S., & Törnqvist, M. (2002). Analysis of acrylamide, a carcinogen formed in heated foodstuffs. *Journal of Agricultural and Food Chemistry,50*(17), 4998–5006. https://doi.org/10.1021/JF020302F

Tsenkova, R. (2009). Introduction aquaphotomics: Dynamic spectroscopy of aqueous and biological systems describes peculiarities of water. *Journal of near Infrared Spectroscopy,17*(6), 303–314. https://doi.org/10.1255/jnirs.869

Tugnolo, A., Giovenzana, V., Malegori, C., Oliveri, P., Casson, A., Curatitoli, M., Guidetti, R., & Beghi, R. (2021). A reliable tool based on near-infrared spectroscopy for the monitoring of moisture content in roasted and ground coffee: A comparative study with thermogravimetric analysis. *Food Control*, 130. https://doi.org/10.1016/j.foodcont.2021.108312

Williams, P. C., & Norris, K. (2001). *Near-infrared technology in the agricultural and food industries* (2nd Ed). Am. Assoc. Cereal Chem.

Wold, S., Ruhe, H., Wold, H., & Dunn, W. J. (1984). The collinearity problem in linear regression. The PLS approach to generalized inverse. *SIAM Journal of Scientific and Statistical Computations,5*, 735–743.

Workman, Jr, J., & Weyer, L. (2007). *Practical guide to interpretive near-infrared spectroscopy*. CRC press. https://doi.org/10.1201/9781420018318

Xie, C., Wang, C., Zhao, M., & Zhao, L. (2023). Prediction of acrylamide content in potato chips using near-infrared spectroscopy. *Spectrochimica Acta Part a: Molecular and Biomolecular Spectroscopy, 301*, 122982. https://doi.org/10.1016/J.SAA.2023.122982

Publisher's Note